Random-Selection-Based Anomaly Detector for Hyperspectral Imagery

Bo Du and Liangpei Zhang

***Abstract*—Anomaly detection in hyperspectral images is of great interest in the target detection domain since it requires no prior information and makes full use of the spectral differences revealed in hyperspectral images. The current anomaly detection methods are susceptible to anomalies in the processing window range or the image scope. In addition, for the local anomaly detection methods themselves, it is difficult to determine the window size suitable for processing background statistics. This paper proposes an anomaly detection method based on the random selection of background pixels, the random-selection-based anomaly detector (RSAD). Pixels are randomly selected from the image scene to represent the background statistics; the random selections are performed a sufficient number of times; blocked adaptive computationally efficient outlier nominators are used to detect anomalies each time after a proper subset of background pixels is selected; finally, a fusion procedure is employed to avoid contamination of the background statistics by anomaly pixels. In addition, the real-time implementation of the RSAD is also developed by random selection from updating data and QR decomposition. Several hyperspectral data sets are used in the experiments, and the RSAD shows a better performance than the current hyperspectral anomaly detection algorithms. The real-time version also outperforms its real-time counterparts.**

***Index Terms*—Anomaly detection, hyperspectral images, multivariate outlier detection.**

I. Introduction

HYPERSPECTRAL imagery, with high spectral resolution, reveals large amounts of detail about the spectral features of the Earth's surface. For example, Airborne Visible/Infrared Imaging Spectrometer (AVIRIS) imagery, which has over 200 bands covering a wide spectral range from 380 to 2500 nm and a spectral resolution of only 10 nm, presents a nearly continuous spectral plot for ground objects. Therefore, minor spectral differences between various materials, which cannot be distinguished in multispectral imagery, can be identified using hyperspectral imagery. Target detection in hyperspectral imagery has been of great interest in the image processing domain for years [1]–[4]. Recently, multilinear algebra, or tensor representation, has been introduced into the target detection domain [5], [6]. It is revealed that tensors integrate the spectral and spatial features of the entire hyperspectral data cube, and the signal can be restored and separated from noise by tensor computation. Detection results from the restored and denoised signals are more promising than those from the original data. However, obtaining prior information about the targets may sometimes be difficult. Therefore, anomaly detection, which does not require prior information about the targets and focuses on distinguishing unusual materials from typical backgrounds without reference to target signatures or target subspaces, drew the attention of researchers in hyperspectral imagery analysis [7]–[12]. Anomalies usually refer to unusual observations or objects in homogenous backgrounds. For example, tanks in a forest background are referred to as anomalies. In anomaly extraction methods, signals are no longer considered separable from noise, but the whole anomaly pixel is assumed to be derived from background statistics [7], [8].

The current anomaly detection methods mainly extract knowledge from the background and use the difference between anomaly targets and the background to detect anomalies. The background refers to nontarget pixels that are predominant in an image compared with target pixels. According to the different ways of extracting knowledge from the background, anomaly detection methods are classified into two main kinds. One assumes that the background is composed of different classes, and the information about these different classes can be estimated from the image, including the probability density function and *a priori* probability. The cluster-based anomaly detector (CBAD) is one example; it detects anomalies in individual clusters after the image scene has been segmented into different clusters [13]. Another example is the multivariate normal inverse Gaussian (MNIG) detector, which assumes that each class fits an MNIG distribution, and the negative log-likelihood of each pixel belonging to its respective class distribution is computed to judge whether a pixel is an anomaly [14]. The other kind considers the background as one single type and acquires the information about the entire background. In this method, the background is assumed to be homogenous in some aspects. The RX algorithm, proposed by Reed and Yu, is typical of this type [15]. The RX algorithm assumes that the background classes have the same multivariate normal distribution, and it uses the sliding window where the center corresponds to the observed pixel and the window is used to calculate background statistics.

Manuscript received February 16, 2010; revised July 5, 2010; accepted September 19, 2010. Date of publication November 11, 2010; date of current version April 22, 2011. This work was supported in part by the National Basic Research Program of China (973 Program) under Grant 2011CB707105, the 863 High Technology Program of the People's Republic of China under Grant 2009AA12Z114, the National Natural Science Foundation of China under Grants 40930532, 40771139, and 40901213, and the Research Fund for the Doctoral Program of Higher Education of China under Grant 200804861058.

B. Du is with the School of Computer, Wuhan University, Wuhan 430072, China, and also with the State Key Laboratory of Information Engineering in Surveying, Mapping, and Remote Sensing, Wuhan University, Wuhan 430079, China (e-mail: gunspace@163.com).

L. Zhang is with the State Key Laboratory of Information Engineering in Surveying, Mapping, and Remote Sensing, Wuhan University, Wuhan 430079, China (e-mail: zlp62@public.wh.hb.cn).

Color versions of one or more of the figures in this paper are available online at http://ieeexplore.ieee.org.

Digital Object Identifier 10.1109/TGRS.2010.2081677

It was first used in multispectral images and later also proved efficient in hyperspectral images, and a subspace version called SSRX was also proposed [7]. The SSRX and RX algorithms are the most widely used methods in anomaly detection and present good performance for anomaly detection in hyperspectral images [7], [8], [15], [16]. However, all the aforementioned anomaly detection methods use all pixels in each local class or image scene to compute background statistics, which is the key background information in anomaly detection. Thus, probable anomalies may also be included in the background covariance matrix, and this can weaken the difference between anomalies and the background. Another problem originates from the local anomaly detector, such as the local SSRX detector. The statistics of the background in these methods are actually computed from the pixels surrounding the observed pixel; hence, the definition of the number of surrounding background pixels is critical. The number of surrounding pixels should be large enough to contain more pixels than the number of bands in order to compute the background covariance matrix inverse. However, a too large number is also undesirable as it may contain anomaly target pixels in the background covariance matrix; this would contaminate the background statistics and reduce the separability of anomalies and the background. Furthermore, a real-time blockwise detector, such as the real-time RX detector, may present false alarms and miss targets as the sliding window moves at the boundary between different backgrounds [17].

Recent research has introduced multivariate outlier detection methods into anomaly extraction from hyperspectral images [18]–[21]. The blocked adaptive computationally efficient outlier nominator (BACON), minimum volume ellipsoid, and minimum covariance determinant (MCD) method are typical ones, which use robust statistics computed from the subsets of the entire hyperspectral data set that is immune to anomalies. Multivariate outlier detection methods present superior performance to traditional benchmark anomaly detection methods, such as the RX and CBAD methods. The reason is that traditional anomaly detection methods use statistics from a contaminated data set, which means that background statistics actually contain anomalies. Smetek and Bauer [19] point out that even as little as 0.5% data contamination would cause obvious covariance distortion. In fact, Smetek and Bauer [19], [21] have established a basis for anomaly extraction by robust statistics, which is the new trend in anomaly extraction from hyperspectral images.

This paper proposes a random-selection-based anomaly detector (RSAD) that randomly selects representative background pixels from an image each time to obtain the background statistics, detects probable anomalies by statistical differences, and, finally, fuses all the detection results. In this way, the RSAD is expected to present better separability between anomalies and the background [1], [3] or lower sensitivity to the contamination by the anomalies and a better performance in the transition areas between different backgrounds.

The remainder of this paper is organized as follows. The RSAD is described in Section II. Section III details the experiments used to test our hypothesis and presents the results of these experiments showing that the RSAD excels in these areas: increased separation between targets and the background, decreased contamination to background statistics by anomalies, improved receiver operating characteristic (ROC) performance, and fewer false alarms in the transitions between different backgrounds. Section IV summarizes this paper.

II. Random-Selection-Based Detector

A. Background Representation

If an anomaly detector is able to suppress the background, the key process is to choose proper features to represent the background. Generally, many anomaly detection methods use the background covariance matrix to carry the background information [10]–[12]. In the RX and SSRX methods, the inverse of the background covariance matrix is used to measure the statistical difference between the observed test pixel, or inner area, and the background. This procedure can be considered as spherizing or whitening of the test vectors with a Gaussian distribution, which produces a random vector with a spherical distribution. Then, the anomaly detection method can be considered as the evaluation of the correlation between the background signature and the test pixel in the whitened space, where both the background and test pixel lie in spherical distributions but with different centers [7]. The background covariance matrix for local detectors is computed from the processing window. As for global detectors, they use all pixels but the ones under detection in the image as the background pixels. As a result, the anomaly pixels contaminate the background covariance matrix.

The aim of the RSAD is to select adequate and representative background pixels from the image scene to compute a proper covariance matrix for the background while restraining the effect of the anomalies. The background pixels are randomly selected to reduce manual intervention. Then, the background statistics from the selected background pixel set are computed for detection purposes.

A number of blocks with the same size are used as the smallest unit of selected background pixels. The following paragraph studies the relationship between N and the probability of striking anomaly pixels.

Suppose the number of anomaly pixels is s and the number of pixels in the complete image is n; then, the probability of striking anomaly pixels when we randomly choose one pixel from the image is s/n. Thus, the probability of striking at least one anomaly pixel in at least one block is represented as

$$P = P'(1) + P'(2) + \cdots + P'(i) + \cdots + P'(N) \quad (1)$$

where $P'(i)$ is the probability of striking i anomaly pixels in all the blocks, and it is considered to be a binomial distribution [22]

$$P'(i) = \frac{N!}{i!(N-i)!} q^i (1-q)^{(N-i)} \quad (2)$$

with $q = 4s/n$, where q is the probability of each chosen block striking the anomaly pixels in the image.

Suppose the number of pixels in the entire image is 10 000 and the number of anomaly pixels is 25. Then, $q = 0.01$. The

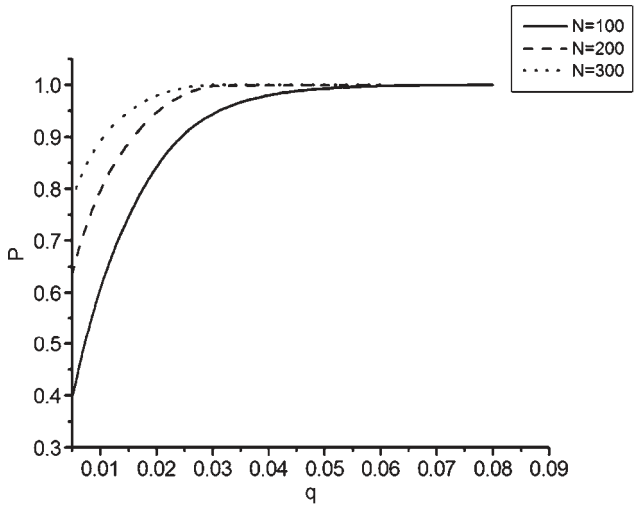

Fig. 1. Relationship between q and P under different values of N.

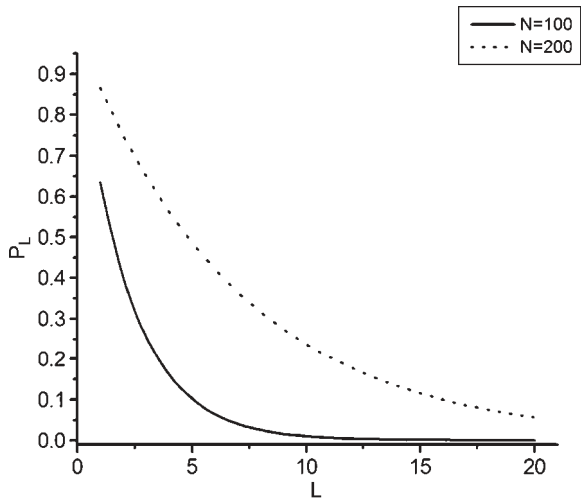

Fig. 2. Relationship between P_L and L under different values of N.

relationship curves between P and q under different N values are shown in Fig. 1. From Fig. 1, it is concluded that, as N increases, the probability of striking anomaly pixels increases sharply. The probability also increases when there are more anomalies or q is larger. It can be concluded that a lower number of blocks are preferred to reduce the probability of striking anomalies in these blocks. However, the number of blocks has to be greater than the number of hyperspectral image bands to make the background covariance matrix invertible.

Since fusion of the detection results is performed after the detection procedures according to each random selection procedure, this paper further studies the probability that all the selections strike anomaly pixels. Suppose that the number of selection procedures is L; then, the probability of all the procedures striking anomaly pixels can be computed as [22]:

$$P_L = P''(i = L) = \frac{L!}{i!(L-i)!} P^i (1-P)^{(L-i)} = P^L \quad (3)$$

where P is equal to that in (1).

The relationship curves between L and P_L are plotted in Fig. 2. Two curves are plotted, both taking the number of anomaly pixels as 25 and the number of blocks as 100 and 200 individually, and the corresponding P is computed from (1). Different curvatures suggest that a larger number of randomly chosen blocks require more procedures of random selection of background pixels. It is obvious that, when L is large enough, the probability of selecting anomaly pixels in these parallel procedures would be dramatically reduced. In this case, the contamination by anomalies in the selected background data set would be minimized so that pixels containing anomalies would be accentuated compared with the background pixels. Combining all the detection procedures according to different random selection procedures, real anomaly pixels should have the largest probability of occurrence and have a comparatively larger intensity in the detection result images. The fusion processing uses this point to extrude anomaly pixels from the background [13].

B. Anomaly Detection and Fusion Procedure

After each random selection procedure, the final pixels representing the background are extracted. Thus, the statistical features of the background can be obtained from them each time. We can then use the statistical features to build the anomaly detector. The detector is assumed to suppress the background and illuminate the anomaly pixels. We use the Mahalanobis-distance-based anomaly detector. Finally, we fuse all the detection results from each detection procedure. The entire procedure is described in the following paragraphs.

N blocks of pixels are selected randomly from the image. N is chosen as a number larger than the number of image bands. Each block contains 2×2 pixels, so there are, in total, $4N$ pixels in the data set of background pixels. These pixels are taken as background representative pixels. Using the data set, the background mean and covariance matrix can be computed. Research in the past decade has proved the effectiveness of the Mahalanobis distance to detect anomalies from their background [23]–[25]. The key assumption of these Mahalanobis-distance-based methods is that the statistical features of the anomalies and background can be depicted by the mean and covariance matrix. Hence, the main difference between these methods is the different ways of computing the mean and covariance matrix of the background. Billor, Hadi, and Velleman proposed the BACON method for multivariate outlier detection in large data sets, and this has become one of the successful outlier detection methods in the applied statistical domain [26]. Recent research has introduced multivariate outlier detection methods to anomaly extraction from hyperspectral images [18]–[21]. Among them, the BACON and the MCD method are typical ones, which use robust statistics for anomaly detection and achieve performance superior to the current benchmark anomaly detection methods [19]. This is because the current anomaly detection methods do not accommodate the effects of outliers, while multivariate outlier detection methods use robust mean and covariance estimates known to be reliable in the presence of outlying observations [20].

The BACON uses an initial subset assumed to be free of anomalies, while the MCD method chooses an initial subset

with the MCD from a series of subsets. Thus, the difference between the MCD method and BACON detector is that the MCD method uses a robust starting point [19]. However, the optimal initial subset in the MCD method may not improve the performance of detection significantly [26]. Moreover, the selected initial subset that is free of anomalies in the BACON might be difficult to determine, while the computational cost is increased. The proposed RSAD does not find an optimal initial subset but has to define the number of random selections. Then, the random selection procedure is performed a sufficient number of times to ensure that at least one constructed subset is free of anomalies. This is much like the MCD method, in which the subsets are randomly selected, among which at least one is assumed to be free of anomalies. The difference is that the RSAD detects anomalies with different subsets' statistics and fuses all the detection results at the last stage, while the MCD method chooses only one subset with the MCD and uses this optimal subset for anomaly detection. Since several subsets may have covariance determinants close to zero, the choosing of such optimal subset is somewhat subjective [27]. In addition, although the randomly selected subsets may not be optimal, the fusion procedure makes the anomaly pixels stand out from the background pixels due to the fact that anomalies would present a high anomalous degree in more detection procedures than nonanomaly pixels would. This is much like the pixel purity index (PPI); the PPI chooses the pixels as end members that have the largest accumulating scores in the projections onto different randomly generated skewers [28]. As a result, the RSAD provides an alternative to the current multivariate outlier detection methods when the optimal initial subset is difficult to determine.

The RSAD uses the same procedure as the BACON to compute the mean and covariance matrix of the background from hyperspectral imagery and finally extract the probable anomalies.

Step 1: Take background pixels, randomly selected using the aforementioned procedure, as the initial basic subset of observed pixels from the hyperspectral imagery. Each observed pixel is virtually a vector containing b' components according to the b' bands.

Step 2: Compute the mean vector and the covariance matrix using the initial basic subset as follows:

$$\overline{\mathbf{x}} = \frac{1}{M}\sum_{i=1}^{M}\mathbf{x}_i \tag{4}$$

$$\mathbf{C} = \begin{bmatrix} \sigma_{11}\sigma_{12}\ldots\sigma_{1b'} \\ \ldots \\ \sigma_{b'1}\sigma_{b'2}\ldots\sigma_{b'b'} \end{bmatrix} \tag{5}$$

where $\sigma_{ij} = (1/M)\sum_k(\mathbf{x}_{ik}-\mathbf{m}_i)(\mathbf{x}_{jk}-\mathbf{m}_j)$, $k = 1,\ldots,M$, M is the number of pixels in the subset, and $\mathbf{m}_i$ and $\mathbf{m}_j$ are the means of the ith band and the jth band, respectively. $\mathbf{x}_{ik}$ is the value in the ith band of the kth pixel.

Step 3: Compute the Mahalanobis distance of each pixel vector in the image using the mean vector and the covariance matrix previously mentioned

$$d_i = \sqrt{(\mathbf{x}_i-\overline{\mathbf{x}})^T\mathbf{C}^{-1}(\mathbf{x}_i-\overline{\mathbf{x}})}, \qquad i = 1,\ldots,M. \tag{6}$$

Step 4: Set the threshold η, and the pixels in the image with a distance under the threshold η would be set as the new basic subset. Reed and Yu have shown that RX statistics under the null hypothesis have a chi-square distribution [15]. The BACON is also a Mahalanobis-based detector and has a chi-square distribution with p degrees of freedom. The threshold is defined as the square root of the $1-\alpha$ percentile of the chi-square distribution with p degrees of freedom. Since the basic subset contains only part of the pixels in the hyperspectral imagery, the square root is multiplied by the inflation factor, which is the same factor as in [26], namely

$$\eta = \chi_{p,\alpha}c_{Npr} \tag{7}$$

where $\chi_{p,\alpha}$ is the square root of the $1-\alpha$ percentile of the chi-square distribution with p degrees of freedom and $c_{\mathrm{Npr}} = c_{\mathrm{Np}} + c_{\mathrm{hr}}$ is the inflation factor

$$c_{\mathrm{hr}} = \max\{0,(h-r)/(h+r)\} \tag{8}$$

$$h = (n+p+1)/2 \tag{9}$$

$$c_{\mathrm{Np}} = 1 + \frac{p+1}{n-p} + \frac{1}{n-h-p} \tag{10}$$

where r is the size of the current basic subset and n is the total number of the pixels in the image.

Step 5: Iterate Step 2 to Step 4 until the basic subset no longer changes.

Step 6: Nominate the pixels excluded by the final basic subset as outliers.

It has been proved that the BACON is computationally efficient for a large data set for it blocks the additional pixels to the basic subset each time, but the number of iterations does not increase with the number of pixels in the basic subset [26]. In addition, it searches for the most reasonable mean vector and the covariance matrix for all the nonanomaly pixels by including new pixels in the basic subsets, which tend to drift toward the real center of nonoutlying background pixels.

The random selection of background pixels and the anomaly detection are repeated L times. Based on the preceding section, we know that repeating the parallel selection and detection procedure several times would remarkably reduce the probability of selecting anomaly pixels as the background in all the procedures. However, the detection results would have to be fused. We use the majority voting rule in the fusion. Each time, we obtain a resulting data set by the BACON anomaly detector according to one random selection of background pixels, nominating each pixel as an anomaly or background.

For each pixel x_l $(l = 1,\ldots,n)$ in the jth $(j = 1,\ldots,L)$ resulting data set, we use the following definitions.

1) If the pixel x_l is judged as a nonanomaly: $\Delta_{0j} = 1$ and $\Delta_{1j} = 0$.
2) Else, if the pixel x_l is judged as an anomaly: $\Delta_{0j} = 0$ and $\Delta_{1j} = 1$.

3) Finally, after all the detection procedures, assign x_l to w_i $(i = 0, 1)$ if $\sum_{j=1}^{L} \Delta_{ij} = \max_{i=0}^{1} \sum_{j=1}^{L} \Delta_{ij}$, where w_0 refers to a nonanomaly pixel and w_1 refers to an anomaly pixel.

C. Real-Time Implementation

Real-time implementation refers to a detection procedure that provides results after the data sample or scanned line arrives at the sensor with a negligible time lag. Real-time implementation has the advantage of processing data online and provides timely analysis to resolve critical situations. There has been an increasing need for the real-time processing of hyperspectral images, particularly in battlefield, reconnaissance and surveillance, environmental monitoring, disaster and damage control, etc. [14]. Research has been carried out on the real-time implementation of the RX and SSRX detection methods [29], [30]. In these real-time detection methods, the sample covariance matrix is replaced by the sample correlation matrix, and the mean would not be removed. In this way, both the first-order and second-order statistics of the images can be taken into account, while the traditional counterpart detectors use only the second-order statistics. Thus, when the target's spectral properties can be solely characterized by the first-order statistics, the real-time detection methods would outperform their traditional counterparts [14]. Moreover, by using QR decomposition, real-time detection methods can be implemented line by line or block by block in the image [30].

We propose a real-time version of the RSAD (RRSAD). In the current real-time detectors, the initial data set used to compute the initial statistics comprises the first blocks or the first lines of the image received by the sensor [31]. In the RSAD, the initial sets of data are also needed. The difference is that we may need more blocks or lines so as to ensure a large enough number of samples for random selection. The procedures for the real-time blockwise RSAD are detailed as follows, and the RSAD can also be implemented in line-by-line real-time processing.

Step 1: Select a pre-fixed number of pixels randomly from the initial blocks or lines of the image to construct the initial subset [31]. If the number of pixels in the initial blocks or lines is less than the pre-fixed number of selection pixels, new blocks or lines scanned by the sensor would be added. The chosen number of the initial blocks obviously affects the performance of the method. On the one hand, a larger number would be necessary for the random selection procedure. On the other hand, a too large number would cause a considerable time lag. However, this time lag can be minimized by choosing the first several blocks or lines with the number of pixels being just greater than the number of spectral bands and randomly selecting just one more pixel than the number of bands for the initial subset. This enables us to avoid the ill-rank singularity problem. For simplicity, we assume that the two blocks contain more than b' pixels, and b' refers to the number of bands in the image. Thus, the optimal initial subset comprises the first two blocks.

Step 2: Compute the statistics from the chosen initial subset and construct the BACON detector. Exclude the pixels from the initial data set that are over the threshold predefined using the method mentioned in the previous section. This BACON detector also utilizes the sample correlation matrix instead of the sample covariance matrix, and the mean no longer has to be subtracted

$$d_i = \left(\mathbf{x}_i^T \mathbf{C}_R^{-1} \mathbf{x}_i\right)^{1/2}, \qquad i = 1, \ldots, n \tag{11}$$

$$\mathbf{C}_R = \frac{1}{M'} \sum_{i=1}^{M'} \mathbf{x}_i \mathbf{x}_i^T \tag{12}$$

where d_i is the detection measurement of the pixel $\mathbf{x}_i$, n is the number of pixels in the image, $\mathbf{C}_R$ is the correlation matrix of the initial subset, and M' is the number of pixels in the initial subset.

Using QR decomposition [32], the inverse of the sample correlation matrix does not need to be computed.

Rewrite the correlation matrix as

$$\mathbf{C}_R = \frac{1}{M'} \sum_{i=1}^{M'} \mathbf{x}_i \mathbf{x}_i^T = \frac{1}{M'} [\mathbf{X}\mathbf{X}^T] \tag{13}$$

where matrix $\mathbf{X}$ is composed of all chosen pixel vectors. $\mathbf{X}$ can be represented by QR decomposition [32], [33]

$$\mathbf{X} = \mathbf{Q}\mathbf{R} \tag{14}$$

where $\mathbf{Q}$ is a unitary matrix and $\mathbf{Q}^T = \mathbf{Q}^{-1}$, $\mathbf{R} = \begin{bmatrix} \mathbf{R}^{\text{upper}} \\ \mathbf{0} \end{bmatrix}$. $\mathbf{R}^{\text{upper}}$ is an upper triangular matrix. $\mathbf{0}$ is a zero vector. The inverse of the sample correlation matrix is expressed as

$$\mathbf{C}_R^{-1} = M'(\mathbf{X}\mathbf{X}^T)^{-1} = M' \left\{ (\mathbf{R}^{\text{upper}})^{-1} \left[(\mathbf{R}^{\text{upper}})^T \right]^{-1} \right\}. \tag{15}$$

Thus, when a new block arrives, we only have to update the matrix $\mathbf{R}^{\text{upper}}$ but do not need to compute the inverse of correlation matrix $\mathbf{C}_R$. That is why the implementation is called a real-time method [30].

Step 3: Update the subset by scanning the new block. The updated subset comprises three parts. One part is the new block. Another part contains the detected anomaly pixels in the last block, if any. The third part consists of the pixels that were randomly selected from the previous scanned blocks with the number equal to that of a block minus the number of anomaly pixels in the last block. The inclusion of the detected anomaly pixels in the last block is to inspect, using the statistics of the updated subset, whether they are real anomaly pixels.

Step 4: Exclude the pixels from the updated subset that are over the pre-fixed threshold, and iterate the detector until the remaining subset no longer changes or the number of iterations reaches three. The limitation on the number of iterations is to ensure the least time lag. Experiments have also shown that, in most cases, the BACON would converge after just a few iterations, and the first iteration would exclude most of the anomaly targets [26].

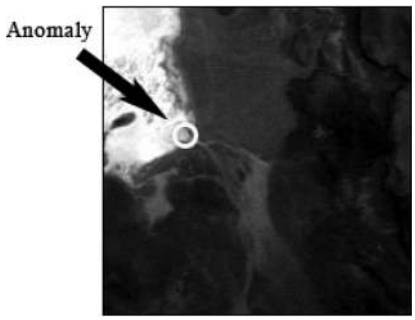

Fig. 3. AVIRIS hyperspectral image.

Fig. 4. Target panels in the AVIRIS image.

Step 5: Iterate Step 3 and Step 4 to scan and detect a new block until the last one of the image, and fuse all the detection results at each detection procedure. In the fusion procedure, only the pixels that are detected as anomalies in both the pixels' block and the neighboring block would finally be considered as anomalies.

III. Experiments and Analysis

A. Separability Analysis

An AVIRIS hyperspectral data set is first used for the separability analysis. Here, the separability refers to the ability of a detector to separate anomalies from the background, particularly when there is contamination of the background statistics by anomalies. The AVIRIS hyperspectral image hereinafter covers the Lunar Crater Volcanic Field in Northern Nye County, NV, downloaded from the National Aeronautics and Space Administration Web site. In our experiment, a subimage was used, which is segmented from the original image and has a size of 200 $\times$ 200. Much research has been performed on the same area [8], [9], [34], and it was revealed that there are five main kinds of background material in the subscene, namely red oxidized basaltic cinders, rhyolite, playa (dry lakebed), shade, and vegetation. A single anomaly containing two pixels in the subscene lies on the border of the dry lakebed in the scene. The single-band image of the data set and the position of the anomaly are shown in Fig. 3.

In the experiment, the atmospheric water bands and low signal-to-noise ratio bands of the data set are removed, reducing the dimension of the image cube from 224 to 120 bands [35]. To make the quantitative analysis possible, 14 target panels are also added to the image, which are shown in Fig. 4. The added targets have the same spectrum as the anomaly pixels previously mentioned but with different sizes. The target panels in the same column have the same size, and from the left to right, their sizes are as follows: 1 $\times$ 2, 2 $\times$ 2, and 1 $\times$ 1. Each column has five similar target panels, and the image with target panels is shown in Fig. 4. In our proposed method, 50 blocks are used to randomly select 200 background pixel vectors each time to ensure the background covariance matrix is invertible. The number of parallel anomaly detection procedures can be determined by the method outlined in Section II and is set to 17 to minimize the probability of striking anomaly pixels.

The global SSRX algorithm [7], [36], BACON, and MCD method are applied as the comparison in the experiment. All these methods use 20 components from principal component analysis transformation to increase the detection efficiency. Fig. 5(a) shows the detection result of the SSRX algorithm on the data set. Fig. 5(b) shows the results of all the detection procedures in our proposed RSAD method before fusion. The 3-D detection results of the BACON and MCD method look similar, so we only show that of the BACON in Fig. 5(c). From Fig. 5(a) and (b), it is found that our proposed method suppresses the background to a much lower range, and the background pixels all lie on a steady range, while the SSRX method outputs the background pixels with stronger fluctuations, with some background pixels presenting high values that would cause false alarms. From Fig. 5(b) and (c), our method presents a similar result to that of the BACON, although the RSAD suppresses the background to a slightly lower range.

To further investigate the separability between targets and the background, we also plotted the output value range of the different detection methods in Fig. 6. In Fig. 6, there are six groups of bars. Each group has a black bar representing the range of the background and a color bar representing the targets. The first group is the detection results by the global SSRX. The second and third groups are the detection procedures with the largest separability and one with the smallest separability in the RSAD, respectively. The fourth group contains the entire accumulative range of the background and targets in all the detection procedures in the RSAD. The last two groups are according to the BACON and MCD method, respectively. From Fig. 6, we can find that the SSRX presents the background with an obviously higher range compared with those of the other detectors. Meanwhile, the targets in the SSRX show a lower and more widespread range than those of the RSAD. The gap between the black bar and the color bar in each group refers to the separability between anomalies and the background for each case. Among these six groups, the second group presents the largest gap. In other words, the RSAD can reveal better separability between anomalies and the background.

To evaluate the final detection performances, the ROC curves are used. These are computed by the detection probability versus false alarm rate. The detector with the best performance is the curve nearest to the upper left, representing the highest detection probability under the same false alarm rates. The ROC curves of the final detection results of the RSAD and the other methods are shown in Fig. 7. In addition, the cluster-based BACON (C-BACON) method [21] is also used this time. It is found that all multivariate outlier detection methods

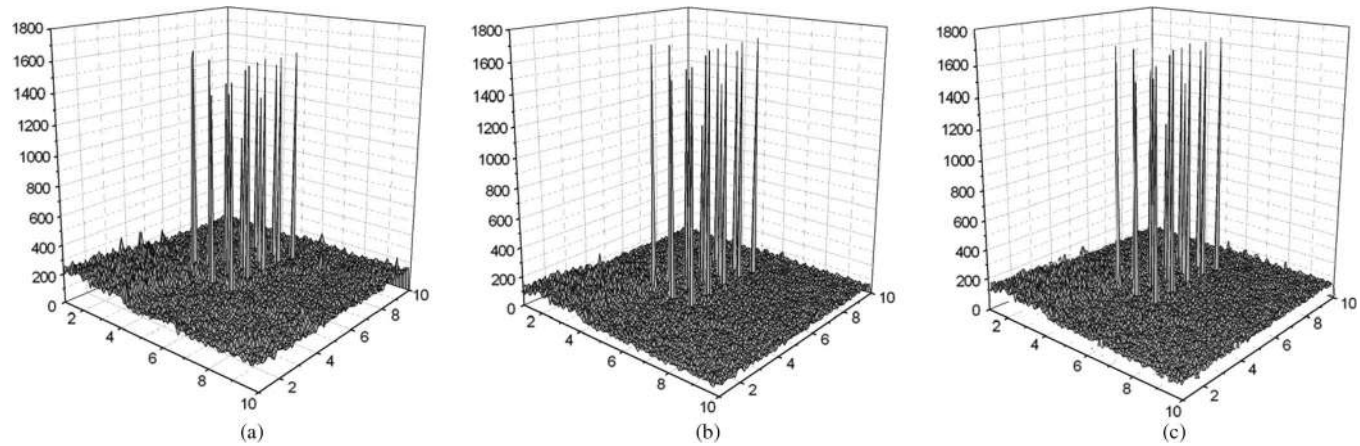

Fig. 5. Three-dimensional plot of detection results. (a) SSRX method. (b) RSAD. (c) BACON.

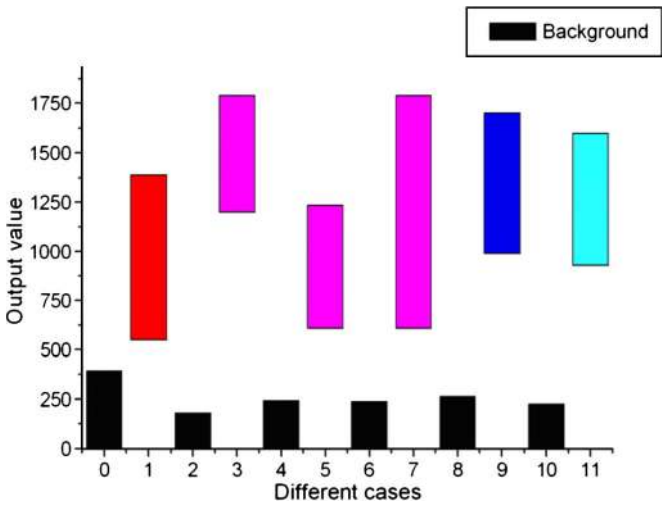

Fig. 6. Separability analysis.

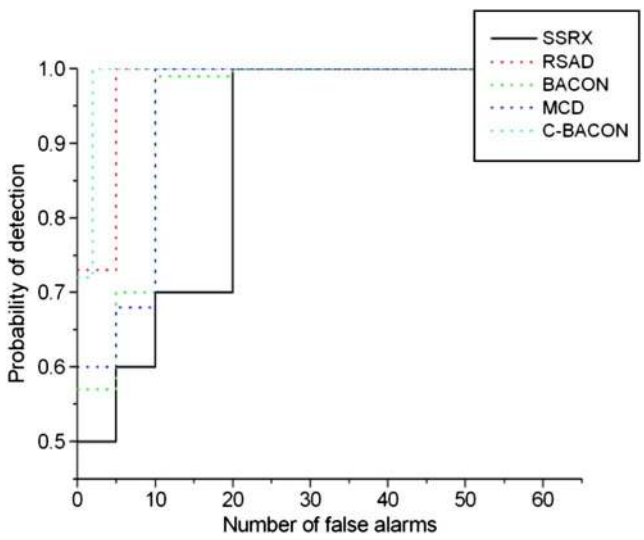

Fig. 7. ROC curves of different detectors.

present better ROC curves than the SSRX method. The RSAD shows a slightly better ROC curve than the BACON and MCD method. However, when the cluster information is taken into consideration, it is proved in Fig. 7 that the C-BACON performs best. The reason is that the backgrounds of the hyperspectral images are from multiple good populations so that applying individual detection to a different background population would be more appropriate [19]. However, the determination of the number of clusters in the hyperspectral images may be somewhat subjective [19]. Furthermore, as the RSAD cannot use the cluster information due to its selection from the whole image, it is fairer to compare it with the multivariate outlier detection methods considering no cluster information. In a word, the RSAD provides an efficient way of using robust statistics to detect anomalies in hyperspectral images with less preprocessing.

Section II has proved that the probability of containing anomaly pixels in all background statistics would be reduced dramatically as the number of parallel detection procedures increases. Anomaly pixels would present a high anomalous degree in most of the parallel detection procedures. Meanwhile, although some background pixels would show a high anomalous degree due to the background statistics deviations such as the false alarms in Fig. 5(a), these background pixels would present a low anomalous degree in most of the parallel detection procedures. Finally, by the fusion strategy of majority voting, anomaly pixels can be accentuated, and false alarms in the individual detection procedures can be suppressed. That is why the RSAD is less sensitive to contamination by the anomalies in the background statistics.

B. Real-Time Detection Experiments

1) Experiments With a Simulated Data Set: In real-time anomaly detectors, the statistics are from the surrounding local areas, resulting in false alarms and missed detection in the areas where block boundaries cross the natural borders between two or more different image backgrounds [17]. Since the RRSAD is based on the statistics of a representative background pixel data set randomly selected each time from the updated pixel data set, it is expected that the RSAD would avoid the sharp change in statistics at the transitions between different backgrounds. Therefore, in this section, we focus on the detection performance at the transitions between different backgrounds. In the experiments, two data sets are used: a simulated hyperspectral data set and a real-world hyperspectral data set. The former

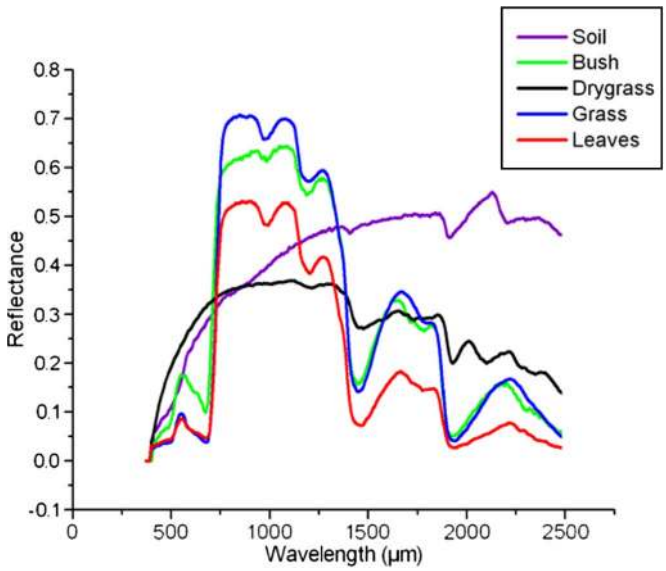

Fig. 8. Spectrum plot of the background materials.

is composed of five kinds of spectrum signatures from the ENVI software spectrum library: grassland soil, coyote bush, dry grass, lawn grass, and blackbrush leaves. The data set has two background regions: One is composed of grassland soil and grass, and the other is composed of bush and leaves. Dry grass is added to the backgrounds and is considered as an anomaly target. The spectrum plots of these five materials are shown in Fig. 8. We calibrated their spectrums to the corresponding bands of AVIRIS data in the overlapping parts of their spectrum and chose 100 bands from 600 to 1800 nm. In this way, we obtained five spectrum signatures, which were vectors with a dimension of 100. Then, using methods similar to those in [2], we obtained the synthetic hyperspectral data set composed of these five spectrum signatures.

The details of the simulated data set are as follows. The data set has 100 bands, and its size is 400 $\times$ 400. Thus, there are 160 000 pixels in the image, which are divided into two parts: The first 200 lines of the image correspond to the background composed of grassland soil and grass, and the remaining 200 lines correspond to the background composed of bush and leaves. Each pixel in the same line has the same composition of background materials. The first line of the image is composed of 100% grass and 0% grassland soil. From the second line, the percentage of grass decreases by 0.25% in each line, and the percentage of soil increases by 0.25% in each line at the same time until the 200th line, where the pixels are composed of 50.25% grass and 49.75% soil. This is the border between the two backgrounds. The above are the pixels of the first background. For the remaining 200 lines of the other background, the synthesizing method is the same. The 201st line is composed of 50% bush and 50% leaves. Then, with a 0.25% increase of bush and a 0.25% decrease of leaves for each line, the 400th line is composed of 99.75% bush and 0.25% leaves. Finally, we replace the background pixels in some positions in the image with the spectrum of dry grass to obtain anomaly pixels, altogether creating ten anomaly targets, five of which are single-pixel ones and five are 2 $\times$ 2. The single-band image of our simulated data is shown in Fig. 9.

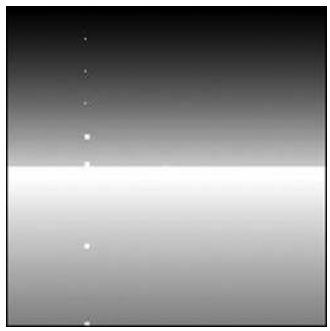

Fig. 9. Single-band image of the simulated data.

Fig. 10. Detection results of the simulated data set. (a) SSRX method. (b) RSAD.

In the experiment, the block size is 10 $\times$ 10, so the image is divided into 1600 blocks. Each time a new block arrives, the updated subset is composed of the new block and a comparable number of randomly selected pixels from the previously scanned blocks and the detected pixels in the last block. This ensures that the pixels detected in the previous block are checked again. A sliding dual concentric window is used in the real-time SSRX. The outer window contains two blocks, and the inner window is 2 $\times$ 2, which is equal to the target size. The detection results of the SSRX and RSAD are shown in Fig. 10(a) and (b), respectively. In Fig. 10(a), it is seen that the SSRX outputs an evident boundary at the transition between the two backgrounds, where the anomalies do not stand out from the boundary. Some anomaly pixels at the transitions between the backgrounds cannot even be identified in the image. In fact, this transition between the different backgrounds is the main source of false alarms. Meanwhile, Fig. 10(b) shows that all the anomaly pixels are separable from the background, and no boundary is apparent in the image. Fig. 11 shows the ROC curves of the two methods, and the RSAD performs much better than the SSRX method: Ours is nearer to the upper-left corner of the coordinate system than the SSRX method. The RSAD keeps the false alarm number to a lower value than the SSRX method under the same detection probability. The improved performance is mainly due to the lower number of false alarms at the transitions between different backgrounds.

The reason for the improved performance is that, in the RSAD, the background statistics for the detector are computed not only from the local areas around the observed pixels but also the pixels randomly selected from the scanned data set, while the SSRX uses local windows around the observed

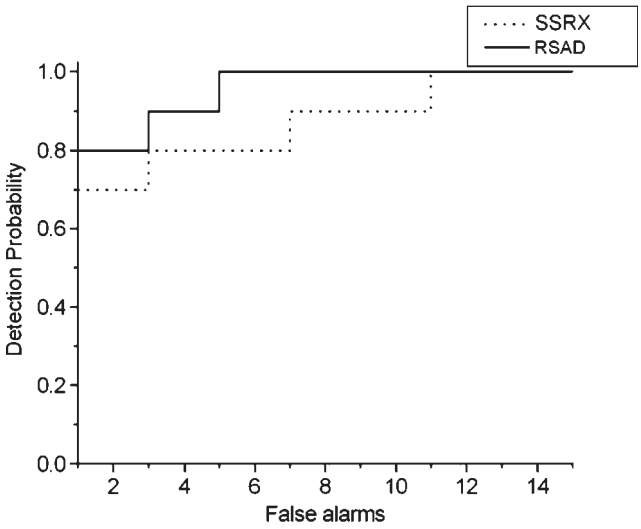

Fig. 11. ROC curves of different detectors.

pixels to select background pixels for the background statistics. When the window slides into the transitions between different backgrounds, the pixels from the background with minority pixels in the window would be statistically different since the majority of pixels come from the other background. As a result, these pixels are the false alarms in the output of the SSRX detector. Although the RSAD may also select the transition areas of the data set, our random selection procedure means that the pixels from one homogeneous background can hardly be dominant in the background statistics. Moreover, the RSAD checks the detected pixels in the next block by the updated and the newly randomly selected data set to reduce the false alarms at the transitions between different backgrounds. Hyperspectral images, particularly the ones scanned vertically to the flight direction, such as the Airborne Real-Time Cueing Hyperspectral Enhanced Reconnaissance hyperspectral data, usually have sharp background transitions. In this case, the RSAD is more practicable.

2) Experiment With a Real-World Data Set: To further evaluate the detection performance at the transitions between different backgrounds, another real-world hyperspectral data set was used. This is an airborne hyperspectral data set from the Reflective Optics System Imaging Spectrometer (ROSIS) optical sensor, which was provided by the Data Fusion Technical Committee of the IEEE Geoscience and Remote Sensing Society. The number of bands of the ROSIS-3 sensor is 115 with a spectral range of 0.43–0.86 μm. The data set has been atmospherically corrected, and some channels have been removed due to noise, with 102 spectral dimensions remaining. We only used the lower part of the image scene with a size of 400 $\times$ 400, as shown in Fig. 12. This subimage contains four obviously different parts of backgrounds from the top to the bottom, which are urban construction area I, river, urban construction area II, and forest area, as shown in Fig. 13.

In the experiment, 18 pixels were chosen from these four transition areas as the anomaly targets, and all are spectrally different from their backgrounds. These anomaly pixels were divided into five groups: The first four groups are from the four different backgrounds previously mentioned, and the last group

Fig. 12. ROSIS image.

Fig. 13. Different background areas.

TABLE I
ANOMALIES IN DIFFERENT BACKGROUNDS

Anomaly Group	Background	Number of anomaly pixels
1	Urban construction area I	4
2	River	6
3	Urban construction area II	2
4	Forest	3
5	Transition of backgrounds	3

is the pixels at the transitions between different backgrounds. The anomaly target pixels in different transitions are detailed in Table I. The spectral plots of different anomalies and those of their background materials are shown in Fig. 14, in which the spectral differences between the anomaly pixels and their backgrounds are obvious. The plots of the backgrounds in the image are the mean spectrum of pixels of the same background. The fifth group of anomaly pixels contains the ones on the boundary of the forest area and construction area II.

The block size was chosen as 10 $\times$ 10, so the image was divided into 1600 blocks. In the RSAD, each time a new block arrives, the updated subset comprises the new block, a comparable number of randomly selected pixels from the previously scanned blocks, and the detected pixels in the last block. This ensures that the pixels detected in the previous block are checked again. A sliding dual concentric window is used in the

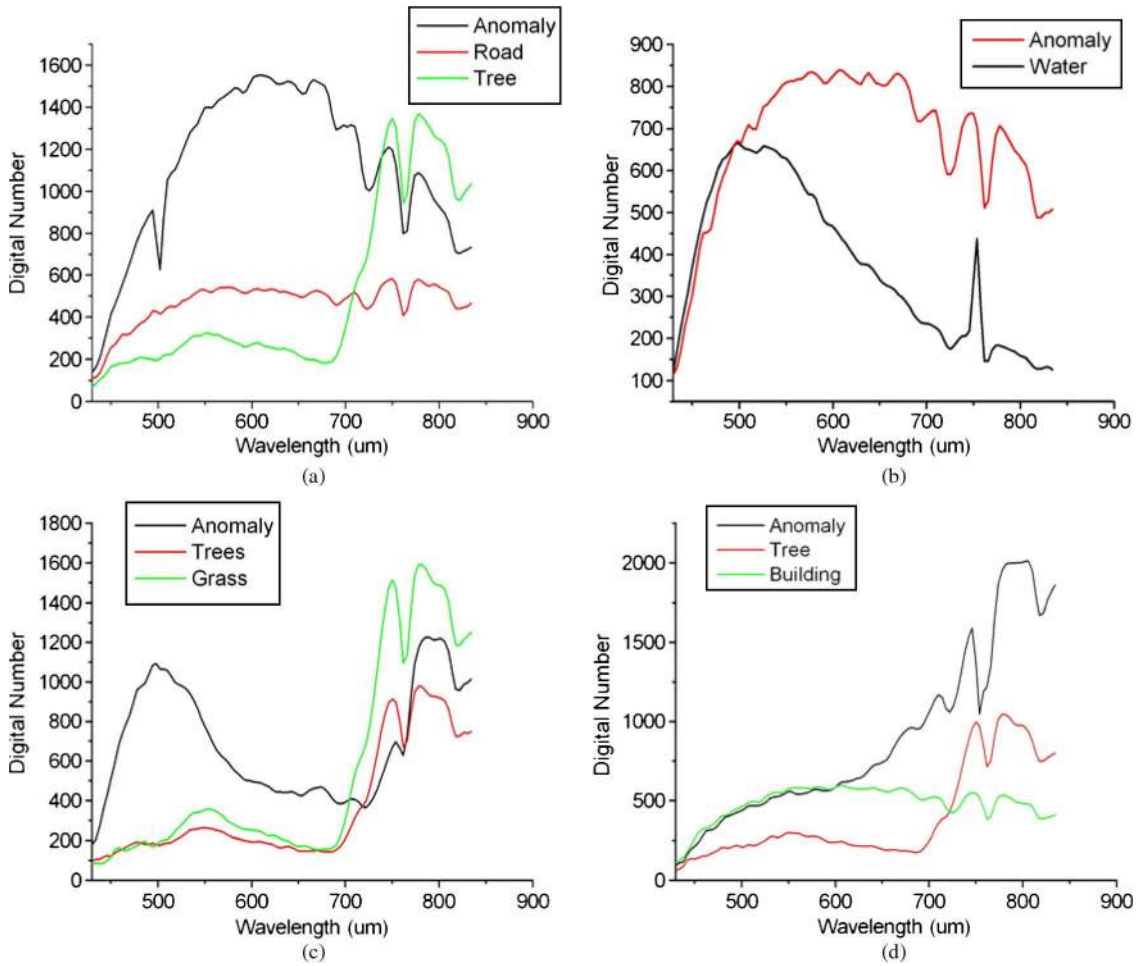

Fig. 14. Spectral plots of different groups of anomalies and their corresponding backgrounds. (a) Anomaly in construction I. (b) Anomaly in river. (c) Anomaly in forest. (d) Anomaly in construction II.

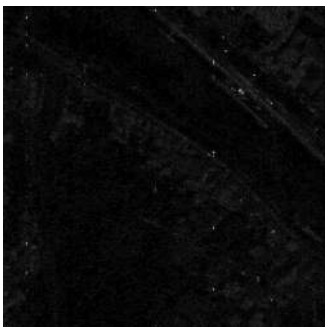

Fig. 15. SSRX detection result image.

Fig. 16. Detection results of RSAD.

SSRX. The outer window contains two blocks, and the inner window is 3×2, which is equal to the largest target size. The result of the SSRX algorithm is shown in Fig. 15. To make the result images comparable, we use the RSAD but with no segmentation, only computing the anomaly degree of each pixel in the image, with which we can finally compute the detection results by threshold segmentation. The anomaly degree image of our detector is shown in Fig. 16. In Fig. 15, there are obvious boundaries between the different backgrounds. Compared with Fig. 15, the boundaries are not so obvious in Fig. 16, and the anomaly pixels are visually more outstanding from their background. To compare the performance quantitatively, the statistics of the SSRX algorithm and our proposed method were calculated by ROC curves in Fig. 17. There is a significant improvement by the RSAD compared with the SSRX algorithm. To further investigate the effect by the boundaries, the detection rate versus the false alarms, appearing on the boundaries of these different backgrounds, is also plotted in Fig. 18. From Fig. 18, it is seen that, compared with our method, the detection performance of the SSRX algorithm is decreased by boundary false alarms.

To analyze the false alarms on the boundary, a subset of our experimental image, segmented from the boundary of the forest area and the construction area, was studied. This subscene is

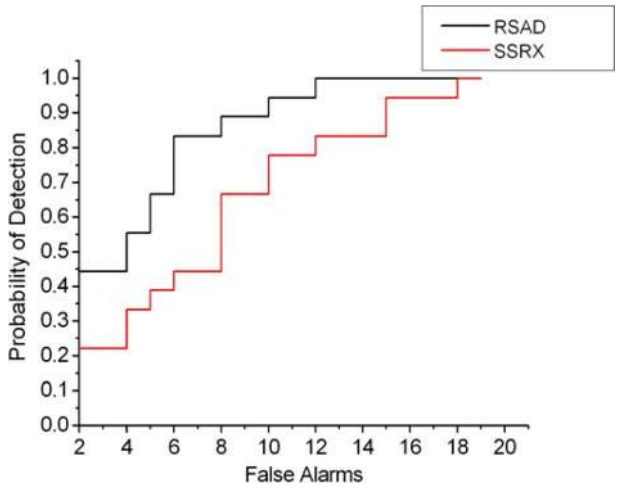

Fig. 17. ROC curves.

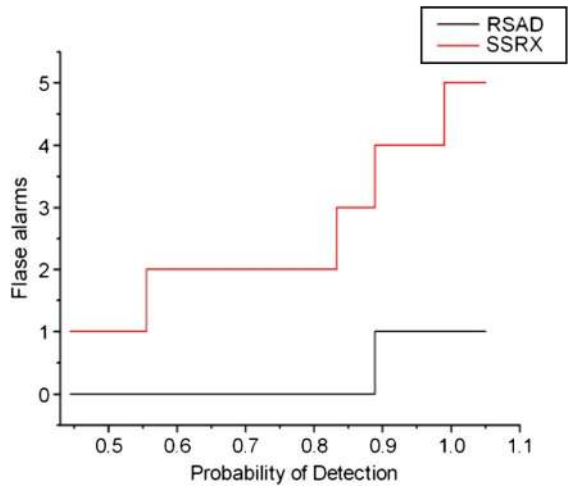

Fig. 18. Detection rate versus false alarms on boundary.

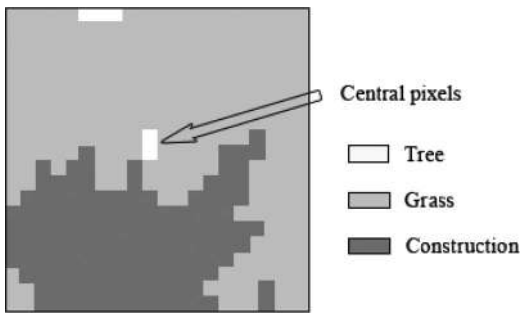

Fig. 19. Subscene of the boundary.

shown in Fig. 19. There are three kinds of background material: tree, grass, and construction, with the former two kinds from the forest area and the latter from construction area II. The two pixels in the center of the scene correspond to a tree. The mean spectral plots of the three materials are shown in Fig. 20. In the SSRX detection results, these central pixels are considered as anomalies due to their sparsity in the sliding window area under the detection procedure. Meanwhile, the RSAD does not present false alarms on these pixels. Trees are widely spread in the image, so in the global scale of the image, they can never be

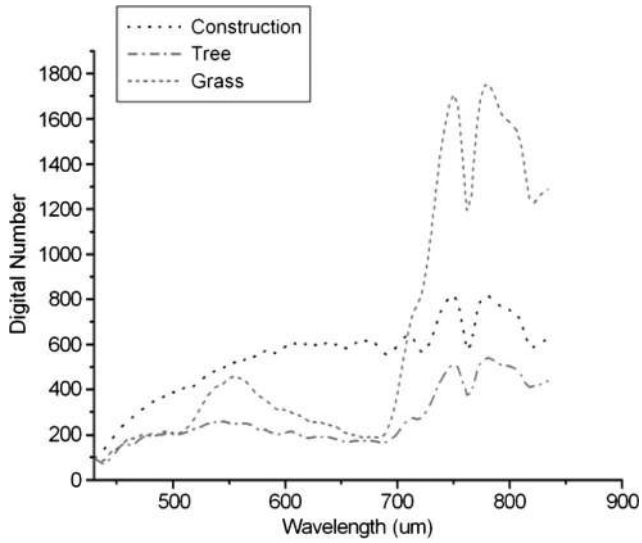

Fig. 20. Spectral plots of the materials in the subscene.

seen as anomalies. In other words, the RSAD takes both local and global statistics into consideration, thereby avoiding false alarms caused by isolated pixels.

IV. Conclusion

This paper has proposed an RSAD for hyperspectral images. This method randomly selects representative background pixels to compute background statistics and reduces the contamination of the background statistics by anomaly pixels by employing a sufficient number of random selections and the fusion of each detection result from the random selections. An RRSAD has also been proposed. The experiments have proven that the RSAD performs better in detecting anomalies compared with the current anomaly detection methods, such as the SSRX algorithm. The RSAD has also presented better separability between anomalies and the background than other successful outlier detection algorithms, such as the BACON and MCD method, when taking no cluster information into consideration. Compared with other real-time anomaly detection methods, the RRSAD can effectively decrease the number of false alarms in the transition areas between different backgrounds and avoid false alarms caused by isolated pixels.

References

[1] D. Manolakis and G. Shaw, "Detection algorithms for hyperspectral imaging applications," *IEEE Signal Process. Mag.*, vol. 19, no. 1, pp. 29–43, Jan. 2002.

[2] C.-I. Chang and D. C. Heinz, "Constrained subpixel target detection for remotely sensed imagery," *IEEE Trans. Geosci. Remote Sens.*, vol. 38, no. 3, pp. 1144–1159, May 2000.

[3] D. Manolakis, D. Marden, and G. A. Shaw, "Hyperspectral image processing for automatic target detection applications," *Lincoln Lab. J.*, vol. 14, no. 1, pp. 79–116, 2003.

[4] L. Zhang, B. Du, and Y. Zhong, "Hybrid detectors based on selective endmembers," *IEEE Trans. Geosci. Remote Sens.*, vol. 48, no. 6, pp. 2633–2646, Jun. 2010.

[5] N. Renard and S. Bourennane, "Improvement of target detection methods by multiway filtering," *IEEE Trans. Geosci. Remote Sens.*, vol. 46, no. 8, pp. 2407–2417, Aug. 2008.

[6] D. Letexier, S. Bourennane, and J. B. Talon, "Nonorthogonal tensor matricization for hyperspectral image filtering," *IEEE Geosci. Remote Sens. Lett.*, vol. 5, no. 1, pp. 3–7, Jan. 2008.
[7] D. W. J. Stein, S. G. Beaven, L. E. Hoff, E. M. Winter, A. P. Schaum, and A. D. Stocker, "Anomaly detection from hyperspectral imagery," *IEEE Signal Process. Mag.*, vol. 19, no. 1, pp. 58–69, Jan. 2002.
[8] C.-I. Chang and S.-S. Chiang, "Anomaly detection and classification for hyperspectral imagery," *IEEE Trans. Geosci. Remote Sens.*, vol. 40, no. 6, pp. 1314–1325, Jun. 2002.
[9] S.-S. Chiang, C.-I. Chang, and I. W. Ginsberg, "Unsupervised target detection in hyperspectral images using projection pursuit," *IEEE Trans. Geosci. Remote Sens.*, vol. 39, no. 7, pp. 1380–1391, Jul. 2001.
[10] H. Kwon and N. M. Nasrabadi, "Kernel RX-algorithm: A nonlinear anomaly detector for hyperspectral imagery," *IEEE Trans. Geosci. Remote Sens.*, vol. 43, no. 2, pp. 388–397, Feb. 2005.
[11] O. Duran and M. Petrou, "A time-efficient method for anomaly detection in hyperspectral images," *IEEE Trans. Geosci. Remote Sens.*, vol. 45, no. 12, pp. 3894–3904, Dec. 2007.
[12] A. Noiboar and I. Cohen, "Anomaly detection based on wavelet domain GARCH random field modeling," *IEEE Trans. Geosci. Remote Sens.*, vol. 45, no. 5, pp. 1361–1373, May 2007.
[13] M. J. Carlotte, "A cluster-based approach for detecting man-made objects and changes in imagery," *IEEE Trans. Geosci. Remote Sens.*, vol. 43, no. 2, pp. 374–387, Feb. 2005.
[14] S. Catterall, "Anomaly detection based on the statistics of hyperspectral imagery," in *Proc. SPIE Conf. Imagery Spectroscopy X*, 2004, vol. 5546, pp. 171–178.
[15] I. S. Reed and X. Yu, "Adaptive multiple-band CFAR detection of an optical pattern with unknown spectral distribution," *IEEE Trans. Acoust., Speech, Signal Process.*, vol. 38, no. 10, pp. 1760–1770, Oct. 1990.
[16] J.-M. Gaucel, M. Guillaume, and S. Bourennane, "Whitening spatial correlation filtering for hyperspectral anomaly detection," in *Proc. Int. Conf. Acoust., Speech, Signal Process.*, 2005, pp. 333–336.
[17] A. V. Kanaev, E. Allman, and J. Murray-Krezan, "Reduction of false alarms caused by background boundaries in real time subspace RX anomaly detection," in *Proc. SPIE—Algorithms and Technologies for Multispectral, Hyperspectral, and Ultraspectral Imagery XV*, S. S. Shen and P. E. Lewis, Eds., Apr. 2009, vol. 7334, pp. 733 405-1–733 405-11.
[18] T. E. Smetek and K. W. Bauer, "A comparison of multivariate outlier detection methods for finding hyperspectral anomalies," *Mil. Oper. Res.*, vol. 13, no. 4, pp. 19–44, 2008.
[19] T. E. Smetek and K. W. Bauer, "Finding hyperspectral anomalies using multivariate outlier detection," in *Proc. IEEE Aerosp. Conf.*, Mar. 2007, pp. 1–24.
[20] J. P. Bellucci, T. E. Smetek, and K. W. Bauer, "Improved hyperspectral image processing algorithm testing using synthetic imagery and factorial designed experiments," *IEEE Trans. Geosci. Remote Sens.*, vol. 48, no. 3, pp. 1211–1223, Mar. 2010.
[21] T. E. Smetek, "Hyperspectral improved anomaly detection and signature matching methods," Ph.D. dissertation, Air Univ., Wright-Patterson AFB, OH, 2007.
[22] J. M. Romano and D. Rosario, "Random sampling statistical analysis for adaptive target-scale-invariant hyperspectral anomaly detection," *Proc. SPIE*, vol. 6565, p. 656 522, May 2007.
[23] H. Viljoen and J. H. Venter, "Identifying multivariate discordant observation: A computer-intensive approach," *Comput. Statist. Data Anal.*, vol. 40, no. 1, pp. 159–172, Jul. 2002.
[24] L. H. Chiang, R. J. Pell, and M. B. Seasholtz, "Exploring process data with the use of robust outlier detection algorithms," *J. Process Control*, vol. 13, no. 5, pp. 437–449, Aug. 2003.
[25] C. Becker and U. Gather, "The masking breakdown point of multivariate outlier identification rules," *J. Amer. Stat. Assoc.*, vol. 94, no. 447, pp. 947–955, Sep. 1999.
[26] N. Billor, A. S. Hadi, and P. F. Velleman, "BACON: Blocked adaptive computationally efficient outlier nominators," *Comput. Statist. Data Anal.*, vol. 34, no. 3, pp. 279–298, Sep. 2000.
[27] A. S. Hadi, "Identifying multiple outliers in multivariate data," *J. R. Stat. Soc., Ser. B*, vol. 54, no. 3, pp. 761–771, 1992.
[28] F. Chaudhry, C. Wu, W. Liu, C.-I. Chang, and A. Plaza, "Pixel purity index-based algorithm to unmix hyperspectral data," in *Recent Adavaces in Hyperspectral Signal and Image Processing*, C.-I. Chang, Ed. Trivandrum, India: Res. Signpost, 2006, ch. 2.
[29] W. Kendall, "The civil air patrol's ARCHER hyperspectral detection system," in *Proc. Specialty Group Camouflage, Concealment, Deception, Mil. Sens. Symp.*, 2005, pp. 17–28.
[30] C.-I. Chang, H. Ren, and S.-S. Chiang, "Real-time processing algorithms for target detection and classification in hyperspectral imagery," *IEEE Trans. Geosci. Remote Sens.*, vol. 39, no. 4, pp. 760–768, Apr. 2001.
[31] A. P. Schaum, "A remedy for nonstationarity in background transition regions for real time hyperspectral detection," in *Proc. IEEE Aerosp. Conf.*, Mar. 4–11, 2006, pp. 1–9.
[32] G. H. Golub and G. F. Van Loan, *Matrix Computations*, 2nd ed. Baltimore, MD: Johns Hopkins Univ. Press, 1989.
[33] C.-I. Chang and M. L. G. Althouse, "A systolic array algorithm and architecture of adaptive spatial filters for FLIR target detection," in *Proc. IEEE Workshop Vis. Signal Process. Commun.*, Hsinchu, Taiwan, Jun. 6–7, 1991, pp. 110–115.
[34] Q. Du, "Optimal linear unmixing for hyperspectral image analysis," in *Proc. IEEE IGARSS*, 2004, vol. 5, pp. 3219–3221.
[35] J. C. Harsanyi and C.-I. Chang, "Hyperspectral image classification and dimensionality reduction: An orthogonal subspace projection approach," *IEEE Trans. Geosci. Remote Sens.*, vol. 32, no. 4, pp. 779–785, Jul. 1994.
[36] B. Stevenson, R. O'Connor, W. Kendall, A. Stocker, W. Schaff, R. Holasek, D. Even, D. Alexa, J. Salvador, M. Eismann, R. Mack, P. Kee, S. Harris, B. Karch, and J. Kershenstein, "The civil air patrol ARCHER hyperspectral sensor system," in *Proc. SPIE—Airborne Intelligence, Surveillance, Reconnaissance Systems and Applications II*, Jun. 2005, vol. 5787, pp. 17–28.

Bo Du received the B.S. degree in graphic engineering and the Ph.D. degree in photogrammetry and remote sensing from Wuhan University, Wuhan, China, in 2005 and 2010, respectively.

He is currently a Postdoctoral Associate with the School of Computer, Wuhan University. His major research interests include pattern recognition, hyperspectral image processing, and signal processing.

Liangpei Zhang received the B.S. degree in physics from Hunan Normal University, Changsha, China, in 1982, the M.S. degree in optics from the Xi'an Institute of Optics and Precision Mechanics, Chinese Academy of Sciences, Xi'an, China, in 1988, and the Ph.D. degree in photogrammetry and remote sensing from Wuhan University, Wuhan, China, in 1998.

He is currently the Head of the Remote Sensing Division with the State Key Laboratory of Information Engineering in Surveying, Mapping, and Remote Sensing, Wuhan University. He is the Principal Scientist for the China State Key Basic Research Project (2011–2016) appointed by the Ministry of National Science and Technology of China to lead the remote sensing program in China. He has more than 200 research papers and is the holder of five patents. His research interests include hyperspectral remote sensing, high-resolution remote sensing, image processing, and artificial intelligence. He is the Editor of several conference proceedings, issues, and geoinformatics symposia. He is also an Associate Editor of *International Journal of Ambient Computing and Intelligence*, *International Journal of Image and Graphics*, *Journal of Geo-spatial Information Science*, and *Journal of Remote Sensing*.

Dr. Zhang is a Fellow of the Institution of Electrical Engineers, an executive member (Board of Governor) of the China National Committee of International Geosphere–Biosphere Programme and the China Society of Image and Graphics, and others. He regularly serves as a Cochair of the series SPIE Conferences on Multispectral Image Processing and Pattern Recognition, Conference on Asia Remote Sensing, and many other conferences. He is recognized as a "Chang-Jiang Scholar" Chair Professor by the Ministry of Education, China.